Springer Handbook of Experimental Fluid Mechanics

B3.7 Sonic Anemometry/Thermometry – Eric R. Pardyjak and Alvaro Cuerva.

Nomenclature

A	Combined rotation matrix
a	Diameter of an ultrasonic transducer
$\bar{a}$	Mean offset error vector
b	Regression coefficients
c	Speed of sound
e	Vapor pressure of water in air
f	Calibration function
i	Cartesian unit vector
j	Cartesian unit vector
k	Cartesian unit vector
L	Distance between sonic transducers
M	Mass
N	Number of Calibration points
P	Combined Rotation matrix
P	Pressure
p	Components of the combined rotation matrix **P**
q	Specific humidity
R	Rotation matrix
S	Rotation matrix
s	Separation distance between the midpoints of pulse paths
T	Rotation matrix
T	Temperature
t	Time
u	Velocity component
u	wind speed vector
$V, \left| \mathbf{u}_\infty \right|, \left| \mathbf{u} \right|$	Magnitude of the wind speed vector
v	Velocity component
w	Velocity component
x	Position coordinate
y	Position coordinate
z	Position coordinate
α	Vertical angle of incidence
β	Acoustic pulse vector angle
δ	Correction in the determination of wind speed.
γ	Ratio of specific heats (C_p/C_v)
λ	Wavelength
ρ	Density
θ	Yaw coordinate rotational angle
φ	Pitch coordinate rotation angle
ψ	Roll coordinate rotation angle

χ Species concentration

Subscripts

1   Coordinate or velocity after first rotation
2   Coordinate or velocity after second rotation
c Corrected
cal Calibration
d Dry air
f Final rotated coordinate system
i Indicates the ith averaging period
m Sonic anemometer, measured coordinate system
min   Minimum
P Projection of the wind speed vector along an acoustic path
pf Planar-fit
w Water vapor
S Sonic
T Incidence angle
v Virtual

Superscripts

$'$ Fluctuating quantity in time
l Linear calibration function
M Measured

Physical and Mathematical Constants

R Gas constant

Operators

$\overline{}$ Average of ensembles, Time average

3.7.1   Introduction & Background

Similar to hot-wire anemometry and LDA, ultrasonic anemometry (or more commonly in the literature sonic anemometry) is a measurement technique that is used to obtain multiple components of instantaneous velocity at a point in space. In addition to the three velocity components, most modern sonic anemometers also provide virtual temperature (T_v^{1}) measurements. Sonic Anemometer/Thermometers (SATs) are very robust: they have no moving parts, require infrequent calibration and can operate in harsh atmospheric environmental conditions. SATs can be left out in the field for extended periods of time

---

[1] In general, the density of air (and the speed of sound) in the atmosphere is dependent on the amount of moisture present. The virtual temperature is the temperature at which dry air has the same density as moist air at the same pressure [3_7.20]. Using this definition, a convenient form of the equation of state may be written as $P=\rho R_d T_v$, where P is total pressure of air including moisture (Pa), ρ is the total density of air (kg/m^3) and R_d is the gas constant for dry air (287 J/(kg-K)) [3_7.48]. The virtual temperature is given by $T_v=T(1+0.61q)$, where T is the absolute temperature. Here, $q=M_w/(M_w+M_d)$ is the specific humidity defined as the ratio of the mass of moist (M_w) air to the total mass of air (M_w+M_d).

with little maintenance compared to hot-wire, cup and propeller anemometers. These qualities combined with the fact that the length and time scales that are resolved with current sonic anemometer technology are quite large (compared to fast response engineering techniques) have made this technique popular with researchers probing the atmospheric boundary layer [3_7.1]. While sonic anemometers are quite robust, the response of sonic anemometers could be affected by intense rain, severe contamination (dirt, dust, etc.), ice formation and structural vibrations. All of these effects are areas of current research efforts [3_7.2]. Table 1 provides a comparison of the main characteristics of the following three traditional atmospheric boundary layer measuring techniques: sonic, cup and propeller anemometers.

System	Calibration	Maintenance	Sampling frequency	3 components of wind speed?	Temperature measurement
Sonic Anemometer-Thermometer	Initial	Cleaning	Up to 100 Hz	Yes (for 3 paths models)	Yes (Sonic Temperature)
	Sonics present some weaknesses that are considered in the text				
Cup Anemometer	Periodic	Intense	Distance constant > 1 m	No	No
	Mobile parts, slow response, influenced by turbulence, influenced by vertical velocity components.				
Propeller Anemometer	Periodic	Moderate	Distance constant > 1 m	Estimate for 3 probe configurations	No
	Mobile parts, slow response, influenced by turbulence and misalignment				

Table 1. Summary of the main operational characteristics of sonic, cup and propeller anemometers.

In recent years, many researchers have used SATs in conjunction with other instrumentation to calculate covariances using the so-called eddy correlation or eddy covariance techniques. The SAT allows for the correlations of velocity components and virtual temperature to be readily computed. For example, useful quantities such as Reynolds stresses ($\overline{u_i' u_j'}$) and turbulent heat fluxes ($\overline{u_i' T_v'}$) are easily calculated from the time series output from the SAT. Additional physical quantities such as the vertical turbulent concentration fluxes of CO_2 and water vapor are regularly measured using this technique [3_7.3] For example, gas sensors can be collocated with the SAT to allow quantities such as $\overline{u_i' \chi'}$ to be calculated (where χ represents the concentration of the tracer gas). As a result of the ability to calculate such useful quantities, SAT use has spread to a variety of applications including air quality [3_7.4, 3_7.5], wind energy [3_7.6, 3_7.7], urban boundary layer [3_7.8, 3_7.9], forest canopy and agriculture [3_7.10], hydrological [3_7.11] and trace gas budget studies (often related to global climate change [3_7.12]). Additionally, SATs have been used as an option for

exploration of extraterrestrial atmospheres [3_7.13, 3_7.14], and low pressure gas anemometry. There is also a flow meter technique based on sonic anemometry [3_7.15].

The type of sonic anemometry described in this section has been used by engineers and micrometeorologists since the late 1950s [3_7.16]. Historically two types of sonic anemometers have been used, pulsed and continuous wave. Pulse anemometers measure time delays between ultrasonic pulses (defined as having frequencies > 20kHz) while continuous wave anemometers measure phase shifts [3_7.17, 3_7.18, 3_7.19]. Using this technology, a SAT measures a "line averaged" velocity of the flow field along the acoustic path. The line averaging represents the main limitation to the instruments frequency response [3_7.20]. Today most manufacturers use pulse based anemometers. Figure 1 shows four different sonic anemometers currently manufactured with varying path lengths and probe configurations.

Fig. 1: Various sonic anemometer configurations: (a) 2D sonic anemometer with vertical mounting base, (b) 3D SAT with vertical mounting base, (c) 3D SAT with horizontal mounting non-orthogonal pulse paths, (d) 3D SAT with horizontal mounting and orthogonal pulse paths. Photographs are courtesy of (a) Vaisala, Inc. (b) RM Young Company, (c) Campbell Scientific, Inc. and (d) Applied technologies, Inc.

3.7.2   Measurement Principles

Most modern sonic anemometers determine velocity components along a known path length by measuring the difference in transit times of acoustic pulses sent simultaneously in opposite directions between two sensors. Multiple paths oriented at various angles allow for measurement of multiple components of the velocity vector. A number of excellent sources exist that describe the fundamental principles of sonic anemometers [e.g., 3_7.17, 3_7.20 and 3_7.21]. For most devices, the ultrasonic pulse is generated using piezoelectric transducers that act as both transmitter and receiver. In some particular cases, when a sonic anemometer is used in other atmospheres (i.e. gases different than air or different conditions leading to different sound speed) the transducer technology may differ. Piezoelectric transducers present an acoustic impedance on the order of $1.2 \cdot 10^7$ kg m^{-2}s^{-1}, whereas the Earth's air presents an acoustic impedance of 400 kg/m^2/s. According to [3_7.13], the ratio of these values makes results in an acceptable attenuation of an ultrasound signal when it is transmitted from a piezo sensor in the Earth's atmosphere. However, for instance in the Martian case, the impedance ratio

would be unacceptable as a result of the extremely low acoustic impedance of the Martian atmosphere (3 kg m^{-2}s^{-1}) would lead to an extreme attenuation of an ultrasound signal transmitted from a piezo sensor. In this case, capacitive transducers with acoustic impedances of 1000 kg/m^2/s can be used as an alternative to piezo transducers.

The description given here is for an ultrasonic pulse type anemometer and is adapted from Kaimal [3_7.17], Kaimal and Finnigan [3_7.10.20] and Cuerva and Sanz-Andres [3_7.21]. The basic principles of operation are best understood by considering a steady, uniform, 2D flow field with an along path velocity component u and the velocity component normal to the path w as shown in Fig. 2. The time of flight for a pulse sent from transducer 1 to traverse to transducer 2 will be denoted t_{12}. Similarly a pulse sent from transducer 2 to 1 will have a time of flight t_{21}. The following equation may be written using the ray vectors shown in Fig. 2 for a pulse being transmitted from sensor 1 to 2:

$$ct_{12} \cos \beta + ut_{12} = L. \tag{1}$$

Here, $\sin \beta = w/c$, c is the speed of sound and L is the distance between transducers 1 and 2. A similar equation may be written for a pulse traveling from sensor 2 to 1. The associated times of flight are then:

$$t_{12} = \frac{L}{c\cos\beta + u} \tag{2}$$

and

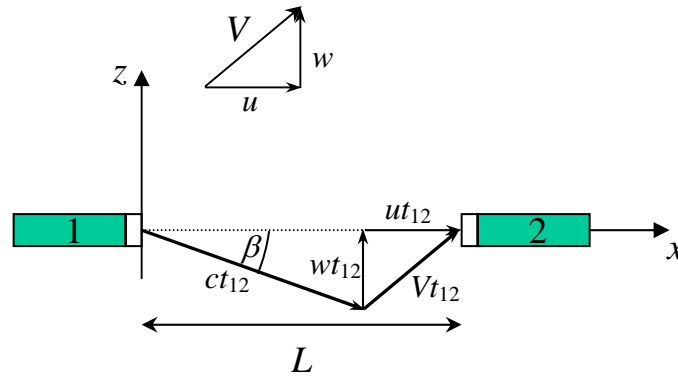$$t_{21} = \frac{L}{c\cos\beta - u}. \tag{3}$$

Fig. 2: 2D schematic of the ray vectors associated with an ultrasonic pulse being sent from the transmitter (1) to the receiver (2) in a steady, uniform velocity field.

The transmitted time difference is then

$$\Delta t = t_{21} - t_{12} = \frac{2uL}{c^2 \cos^2 \beta - u^2} .$$

(4)

Substituting $\sin^2 \beta + \cos^2 \beta = 1$ and $u^2 + w^2 = V^2$ gives

$$\Delta t = \frac{2uL}{c^2 - V^2} .$$

(5)

For small Mach number flow, $V \ll c$ the along path wind component simplifies to

$$u = \frac{c^2}{2L} \Delta t .$$

(6)

Eq. (6) requires the speed of sound to be estimated. Following [3_7.17], the effect of temperature and water vapor content can be accounted for by approximating the speed of sound as $c^2 = C_T T(1 + 0.32\, e/P)$, where T is the absolute temperature (K), e is the vapor pressure of water in air and P is the atmospheric pressure. The virtual temperature is approximated as $T_v = T(1 + 0.32\, e/P)$ so that $c^2 = C_T T_v$. This can be related to the familiar definition of the speed of sound given by $c^2 = \gamma P/\rho$, where $\gamma = C_p/C_v$ is the ratio of specific heats at constant pressure and volume and ρ is the density of air (kg/m^3). Substituting the ideal gas relationship with the virtual temperature (see footnote 1), $P = \rho R_d T_v$, yields $c^2 = \gamma R_d T_v$.

Most SATs however, use a single path to simultaneously send pulses from sensor 1 to 2 and 2 to 1 respectively. These instruments use electronics to subtract time inverses directly, namely:

$$\frac{1}{t_{12}} - \frac{1}{t_{21}} = \frac{2u}{L} .$$

(7)

This yields the velocity along the path without the need to separately calculate the speed of sound. The resulting equation for the velocity is simply

$$u = \frac{L}{2}\left(\frac{1}{t_{12}} - \frac{1}{t_{21}} \right).$$

(8)

It should be noted that, in a real configuration, the pulses are not sent simultaneously because of physical limitations (it is technically impossible for a sensor to act as both an emitter and receiver simultaneously). In practice there is a time delay between shots (z_B) that is on the order of 0.001 s depending on the manufacturer. The effect of this time delay between pulses must be taken into account when a sonic anemometer measures the turbulence velocity and temperature spectra [3_7.21].

6

As shown in Kaimal and Finnigan [3_7.20] the time inverses method also allows the speed of sound to be calculated directly, hence providing an estimate of virtual temperature. Squaring the sum of the inverse flight times yields,

$$\left(\frac{1}{t_{12}}+\frac{1}{t_{21}}\right)^2 = \frac{4c^2}{L^2}\cos^2\beta = \frac{4c^2}{L^2}\left(1-\frac{w^2}{c^2}\right).$$ (9)

Eq. (9) can then be solved for the speed of sound,

$$c^2 = \frac{L^2}{4}\left(\frac{1}{t_{12}}+\frac{1}{t_{21}}\right)^2 + w^2.$$ (10)

Using the approximation derived above, $c^2 = C_T T_v$ yields the following expression for the virtual temperature:

$$T_v = \frac{L^2}{4C_T}\left(\frac{1}{t_{12}}+\frac{1}{t_{21}}\right)^2 + \frac{w^2}{403}.$$ (11)

For a multi-component anemometer, w in Eq. (11) can be calculated using the velocity components from the other axes of the anemometer. The exact formulation for w depends on the geometry of the SAT axes. This temperature is actually the sonic temperature (the temperature reported by the SAT) but for most applications represents the virtual temperature quite well [3_7.22]. As noted by [3_7.23], most SATs actually determine sonic temperature as an average over multiple paths. In that case, Eq. (11) represents the sonic temperature obtained for one path.

Activated Path	1	1	2	2	3	3	Electronic and computation
Path Sense	1-2	2-1	1-2	2-1	1-2	2-1	
Time [ms]	z_B 1.14	z_B 1.14	z_B 1.14	z_B 1.14	z_B 1.14	z_B 1.14	z_E 0.88

Table 2. Pulse sequence and timing for a METEK USA-1 sonic anemometer. The Activated Path refers to the paths shown in Fig. 3, while the Path Sense refers to the transmitter to receiver communication shown in Fig.2.

For a three path sonic anemometer (e.g. Fig. 3), a full sequence leading to a complete measurement of the wind speed vector comprises at least six shots of ultrasound pulses, two pulses per acoustic path. The time required for computing the wind speed vector

from individual path measurements is limited by a time delay z_B between consecutive pulses and a time after the sixth pulse z_E for resetting the electronics. Table 2 shows a typical pulse sequence which lasts $6\,z_B + z_E = 7.72$ ms [3_7.24].

In general, SATs do not provide the direct measurements from the individual pulse sequence. Instead they carry out averaging processes on them. These processes, normally called "block averaging", are manufacturer dependent. A typical scheme of such processes is included in Table 3.

Path	Pulse Sense	Start time	End time
Path 1	1-2	0	z_B
Path 1	2-1	z_B	$2z_B$
Path 2	1-2	$2z_B$	$3z_B$
Path 2	2-1	$3z_B$	$4z_B$
Path 3	1-2	$4z_B$	$5z_B$
Path 3	2-1	$5z_B$	$6z_B$
Mode	Averaged Measurements	Final number of averaged measurements delivered (true number of samples per second)	
1	8	21 (168/8)	
2	3	56 (168/3)	

Table 3. Typical Pulse firing sequence and block averaging for a Gill Wind Research sonic anemometer. Time delay between pulses z_B=0.001 s. Data delivering speed 168 samples/s.

3.7.3 Device Characteristics, Accuracy and Limitations

Most SATs attributes vary across manufactures. Typical sensor measurement paths are approximately 0.10-0.20 m. The velocity range of most sensors is approximately ± 30 m s^{-1} with velocity accuracies in the range of ± 0.02 to ± 0.05 m s^{-1}. Temperature accuracy tends to vary much more significantly over a range of ± 0.1 to $\pm 2.0\,^{\circ}$C. The sampling frequency range is typically up to about 100Hz. Some manufactures also allow for oversampling of wind components and output an average filtered signal at a lower frequency as discussed above via a block averaging process (see Table 3).

The frequency response of a SAT is limited by the attenuation in spatial response imposed by line averaging along a path. Kaimal [3_7.20] and Kaimal and Finnigan [3_7.20] have suggested as a "rule of thumb" that the low pass filtering attenuation distortions are confined to spectral wavelengths $\lambda < 2\pi L$. If the paths of sensors are separated (e.g., non-intersecting paths as in Fig. 1d) then, the response of the turbulent fluxes (e.g., $\overline{u_i'T_v'}$ or $\overline{u_i'u_j'}$) calculated between the sensors is compromised if $\lambda < 2\pi s$, where s is the separation distance between the midpoints of the pulse paths. For a typical SAT with intersecting sensor paths and a sensor separation of $L = 0.10$ m (e.g., Fig. 1c), spectral attenuation will occur for wavelengths less than about 0.63 m. Using Taylor´s

frozen turbulence hypothesis to express this limit in terms of frequency for L=0.1 m and a typical wind speed u=10 m/s leads to a limiting frequency $f=u/(2\pi L)\approx15.9$ Hz).
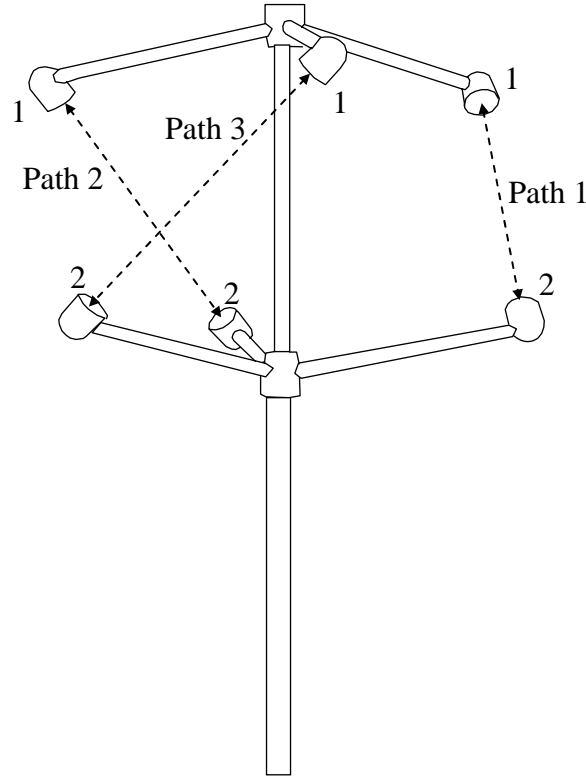

Fig. 3: Schematic of a commercial 3D sonic anemometer indicating the three pathlines.

These "rules of thumb" were developed assuming a homogeneous turbulent velocity field [3_7.25]. Cuerva et al. [3_7.21] have investigated the effect of this assumption on measurements made on more realistic flow fields. In particular, they investigated line averaging effects for a non-steady, non-uniform velocity field through the sensor. They found that the flow Mach number and the time delay between pulses increases the wavelength at which spectral attenuation begins. In some cases, the combination of line averaging and geometry effects leads to overestimation of the spectra instead of to spectral attenuation.

As a result of the line averaging, care must be taken when placing the sensors near surfaces. For use in the atmospheric surface layer, the minimum distance between the center of the probe and the ground has been suggested to be $z_{min}=8\pi L$ [3_7.26]. Wamser et al. [3_7.27] however, showed that the maximum attenuation occurs in the vertical velocity variance near the ground and that the z_{min} restriction can be relaxed down to about $z_{min}=4L$ or just less than one meter for most SATs over flat terrain. Additionally, depending on the application, the block averaging process can lead to non-negligible effects of the determination of turbulence properties [3_7.28], [3_7.29].

The effect of aerodynamic disturbances associated with the acoustic path supporting structures on the measurement of averaged characteristics of the wind speed vector must be considered. This effect is highly manufacturer dependent [3_7.30]. Figure 4 shows the corrections in the measurement of the average value of the total magnitude of the wind speed as function of the angle of incidence of the wind speed vector for a commercial sonic anemometer unit. These corrections are easily determined by a calibration process and can be implemented internally (by the manufacturer) or during post processing by the user.
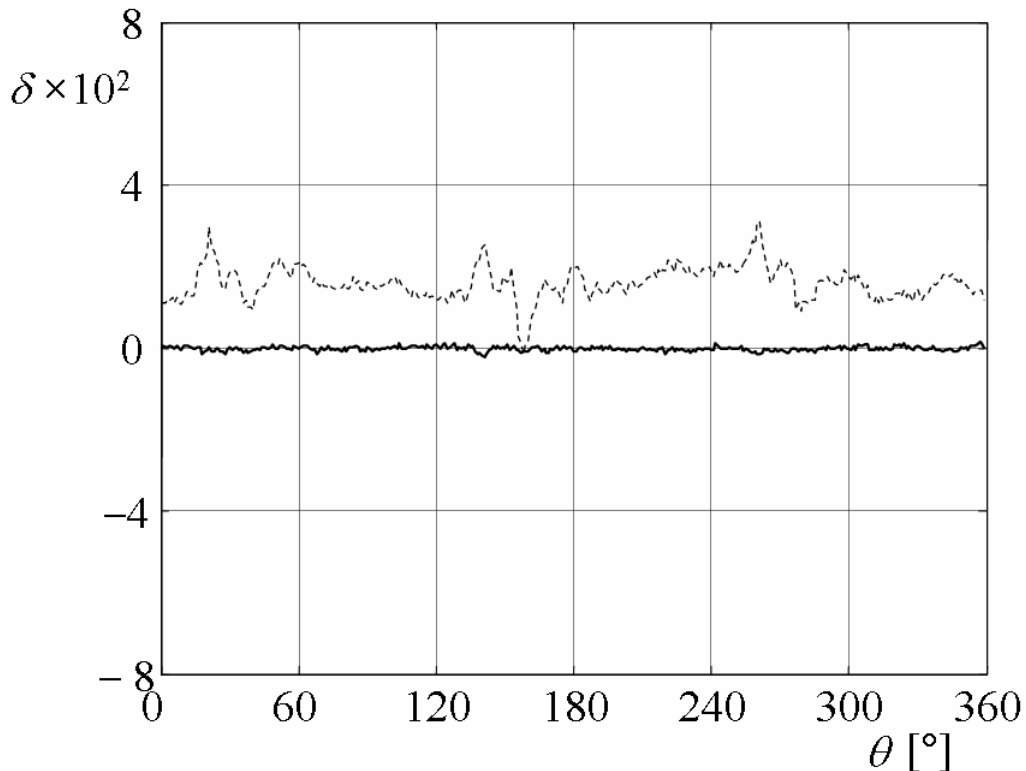
Fig. 4: Difference between the measured wind speed magnitude $|u|^M$ and the actual magnitude $|u|$ as a percentage of the actual one (represented as δ) versus the incidence angle θ. The dotted line represents the un-corrected response (it is bounded by 0% and 3%) of the anemometer and the solid line the corrected response after calibration in wind tunnel [3_7.31].

In general, it can be stated that these two phenomena: 1) supporting structures aerodynamic interference on the acoustic paths and 2) the line averaging process make the sonic anemometer response non-isotropic (i.e. directional), both when measuring averaged and turbulent magnitudes. The characteristics of this directional response depend on the sensor design.

3.7.3.1 Coordinate Transformation Methods

The alignment of a SAT is of great importance since misalignment produces a deviation between the assumed probe coordinate system and the actual one. SATs are often aligned in the field such that the *y*-axis points northward, the *x*-axis eastward and *z*-axis normal to the surface. Another common horizontal alignment technique is to orient the anemometer in manner that limits flow distortion as much as possible based on the expected winds. Alignment is typically accomplished using tools such as inclinometers, compasses, global positioning units, and levels. Unfortunately, some level of misalignment is unavoidable and causes the various components of the velocity field to be incorrectly redistributed. As noted by [3_7.32], this can be particularly problematic when calculating velocity covariances over sloping terrain where the SAT is usually either aligned with the vertical component normal to the slope or leveled. Wilczak et al. [3_7.32] review several correction/coordinate transformation algorithms that are useful for sonic anemometers. Following [3_7.32], [3_7.20] and [3_7.33] the most widely used coordinate transformation technique is presented below followed by Wilczak et al.'s [3_7.32] alternative method. These methods transform velocities in the measured coordinate system into a streamline coordinate system. This operation is very useful for comparing wind tunnel data or theory to atmospheric surface layer data. It is also particularly useful for investigating turbulent surface exchanges such as the turbulent vertical flux of momentum or a scalar (e.g., $\overline{u_i'\chi'}$ or $\overline{u_i'u_j'}$). The coordinate transformations are most appropriate over horizontally homogeneous, uniformly sloping terrain (e.g., in inertial layer above forests, buildings, fields, etc.).
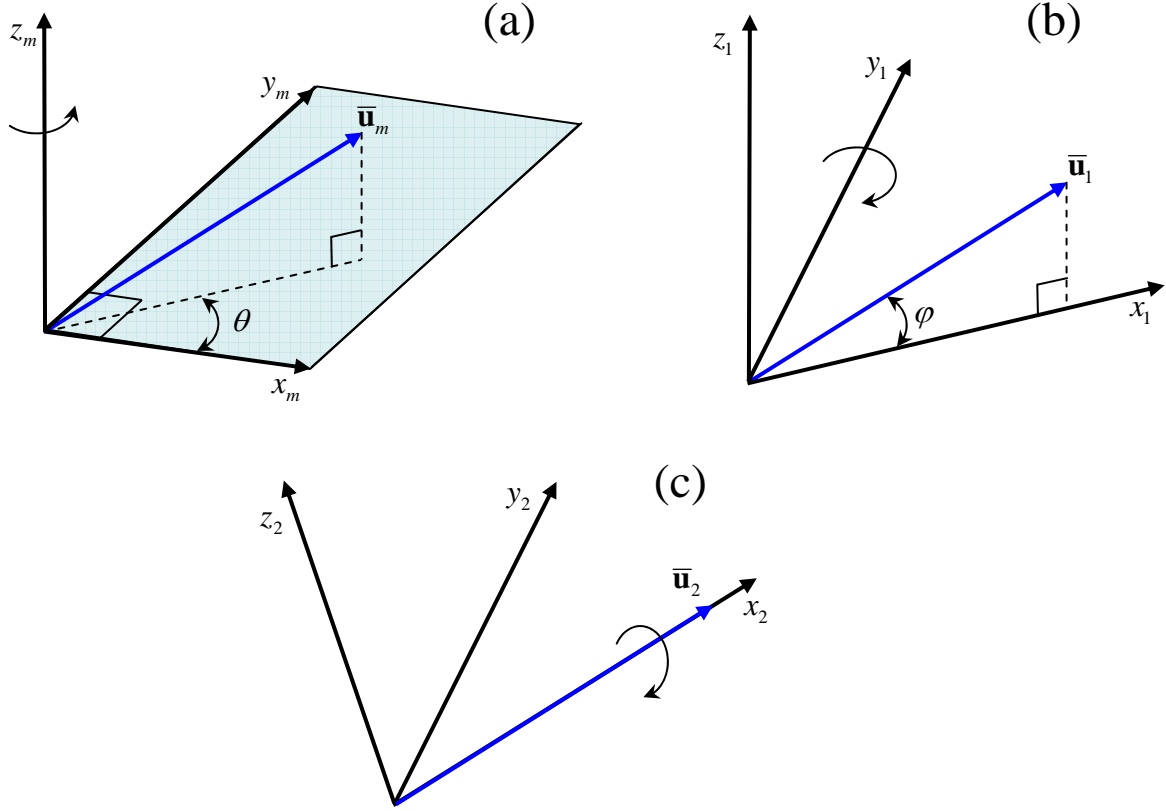
Fig. 5: Schematic of the coordinate rotation technique showing the first rotation about the (a) z_m axis (yaw), (b) the second rotation about the y_1 axis (pitch) and the final rotation about the x_2 axis (roll). $\overline{\mathbf{u}}_m = (\overline{u}_m, \overline{v}_m, \overline{w}_m)$, $\overline{\mathbf{u}}_1 = (\overline{u}_1, 0, \overline{w}_1)$, $\overline{\mathbf{u}}_2 = (\overline{u}_2, 0, 0)$ are the average velocity vectors referred to in the sonic anemometer coordinate system (x_m, y_m, z_m), after the first rotation with a reference system (x_1, y_1, z_1), and second rotation with a reference system (x_2, y_2, z_2) respectively.

A transformation of the measured coordinate system into a streamline coordinate system is a transformation between two orthogonal coordinates systems and is shown schematically in Fig. 5. This is a rotation operation that can be represented in matrix form as:

$$\begin{bmatrix} u_f \\ v_f \\ w_f \end{bmatrix} = \mathbf{A} \begin{bmatrix} u_m \\ v_m \\ w_m \end{bmatrix} \tag{12}$$

$$\mathbf{A} = \mathbf{T} \cdot \mathbf{S} \cdot \mathbf{R},$$

where, u_m, v_m, w_m are the instantaneous velocity components in the measured sonic coordinate system and u_f, v_f, w_f are the final instantaneous velocity components after the

12

transformation. As noted by Sozzi [3_7.33], a method to obtain an approximation of **A** is to combine one or more rotations in order to align the coordinate system axes in which the measurements where made (x_m, y_m, z_m with unit vectors $\mathbf{i}_m$, $\mathbf{j}_m$, and $\mathbf{k}_m$) with the tangent, binormal and principal normal of the local streamline (x_f, y_f, z_f with unit vectors $\mathbf{i}_f$, $\mathbf{j}_f$, and $\mathbf{k}_f$) as shown in Fig. 6 using:

$$\mathbf{T} = \begin{bmatrix} 1 & 0 & 0 \\ 0 & \cos\psi & \sin\psi \\ 0 & -\sin\psi & \cos\psi \end{bmatrix} \mathbf{S} = \begin{bmatrix} \cos\varphi & 0 & \sin\varphi \\ 0 & 1 & 0 \\ -\sin\varphi & 0 & \cos\varphi \end{bmatrix} \mathbf{R} = \begin{bmatrix} \cos\theta & \sin\theta & 0 \\ -\sin\theta & \cos\theta & 0 \\ 0 & 0 & 1 \end{bmatrix}.$$

Here, ψ, φ and θ are the roll, pitch and yaw rotation angles respectively taken as positive counterclockwise about each axis. The principal normal is defined by the direction in which the streamline is curving most rapidly [3_7.20]. Often times, in practice, the estimation procedure is further simplified with a rougher estimate that only consists of the first two rotations or the so-called double rotation, first about the z_m axis and then the y_1 axis.
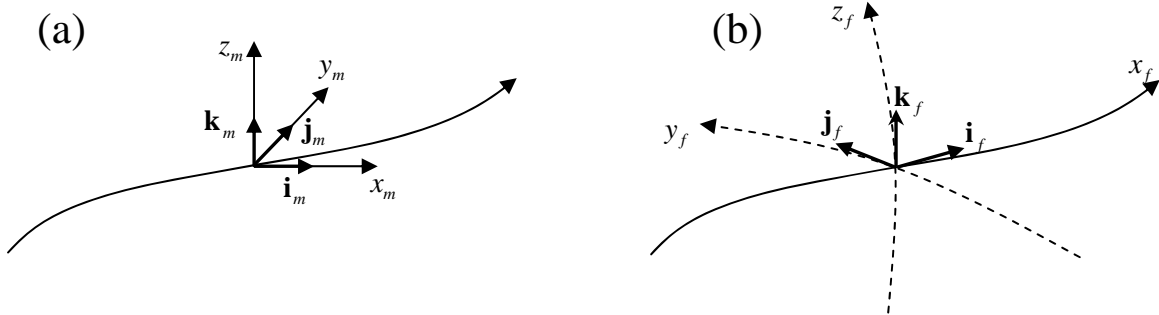

Fig. 6: Schematic of (a) a streamline passing through the sonic anemometer coordinate system and (b) the streamline coordinate system as discussed in the text (adapted from [3_7.34]). $\mathbf{i}_f$ is tangent to the streamline, $\mathbf{j}_f$ binormal to the streamline and $\mathbf{k}_f$ normal to the streamline. As noted by Finnigan [3_7.34] the z_f coordinate lines are tangent to the field of $\mathbf{k}_f$ vectors, the y_f coordinate lines are tangent to the field of $\mathbf{j}_f$ vectors and the streamlines form the x_f coordinates.

The procedure is typically broken up into three rotation operations. If x_m, y_m, z_m is the measuring coordinate system of the sonic anemometer, the first operation is a rotation about the vertical (z_m) axis that aligns the new x-coordinate with the mean streamwise wind direction, i.e., $[x_m, y_m, z_m] \rightarrow [x_1, y_1, z_1]$ so that the mean spanwise velocity is zero. That is,

$$\begin{bmatrix} u_1 \\ v_1 \\ w_1 \end{bmatrix} = \mathbf{R} \begin{bmatrix} u_m \\ v_m \\ w_m \end{bmatrix} \text{ or,}$$

$$u_1 = u_m \cos\theta + v_m \sin\theta$$
$$v_1 = -u_m \sin\theta + v_m \cos\theta \tag{13}$$
$$w_1 = w_m$$

where,

$$\theta = \tan^{-1}\left(\frac{\bar{v}_m}{\bar{u}_m}\right), \qquad \sin\theta = \frac{\bar{v}_m}{\sqrt{\bar{u}_m^2 + \bar{v}_m^2}} \quad \text{and} \quad \cos\theta = \frac{\bar{u}_m}{\sqrt{\bar{u}_m^2 + \bar{v}_m^2}}.$$

In the above equations, $\bar{v}_m$ and $\bar{u}_m$ are mean velocities in the measured sonic anemometer coordinate system. Therefore, the transformation is based on the choice of the mean velocity. This should be an ensemble average, however, practically it is usually estimated with time averages. After the first rotation, $\bar{v}_1 = 0$ by definition. Once θ is determined, either the time series can be rotated using (13) or the following equations for mean flow and turbulent stresses can be used:

$$\overline{u_1} = \overline{u_m} \cos\theta + \overline{v_m} \sin\theta$$
$$\overline{v_1} = -\overline{u_m} \sin\theta + \overline{v_m} \cos\theta \tag{14}$$
$$\overline{w_1} = \overline{w_m}$$

$$\overline{u_1'^2} = \overline{u_m'^2} \cos^2\theta + \overline{v_m'^2} \sin^2\theta + 2\overline{u_m' v_m'} \sin\theta \cos\theta$$
$$\overline{v_1'^2} = \overline{u_m'^2} \sin^2\theta + \overline{v_m'^2} \cos^2\theta - 2\overline{u_m' v_m'} \sin\theta \cos\theta \tag{15}$$
$$\overline{w_1'^2} = \overline{w_m'^2}$$

$$\overline{u_1' v_1'} = \overline{u_m' v_m'}\left(\cos^2\theta - \sin^2\theta\right) + \sin\theta \cos\theta\left(\overline{v_m'^2} - \overline{u_m'^2}\right)$$
$$\overline{u_1' w_1'} = \overline{u_m' w_m'} \cos\theta + \overline{v_m' w_m'} \sin\theta \tag{16}$$
$$\overline{v_1' w_1'} = -\overline{u_m' w_m'} \sin\theta + \overline{v_m' w_m'} \cos\theta$$

As shown in Fig. 5b, the second rotation is about the y_1 axis and forces $\overline{w_2} = 0$. The velocities are given by

$$u_2 = u_1 \cos\varphi + w_1 \sin\varphi$$
$$v_2 = v_1 \tag{17}$$
$$w_2 = -u_1 \sin\varphi + w_1 \cos\varphi$$

where,

$$\varphi = \tan^{-1}\left(\frac{\overline{w_1}}{\overline{u_1}}\right), \tag{18}$$

$$\sin \varphi = \frac{\overline{w}_1}{\sqrt{\overline{u}_1^2 + \overline{w}_1^2}} \quad \text{and}$$

$$\cos \varphi = \frac{\overline{u}_1}{\sqrt{\overline{u}_1^2 + \overline{w}_1^2}} .$$

Equations similar to (14)-(16) can then be easily obtained. This completes the double rotation and aligns x_2 with the mean wind direction. The last rotation or triple rotation rotates the coordinate system such that the final z-axis is normal to the mean wind trajectory [3_7.33] (See Fig 4b). According to [3_7.32] there are an infinite number of rotations that satisfy $\overline{v}_f = \overline{w}_f = 0$. [3_7.35] and [3_7.20] suggest that the following approximation be made over flat land: $\overline{v'_f w'_f} = 0$. If this is done, the following equations result:

$$
\begin{aligned}
u_f &= u_2 \\
v_f &= v_2 \cos \psi + w_2 \sin \psi \\
w_f &= -v_2 \sin \psi + w_2 \cos \psi
\end{aligned}
\qquad , \tag{19}
$$

where,

$$\psi = \frac{1}{2} \tan^{-1} \left(\frac{2 \overline{v'_2 w'_2}}{\overline{v'^2_2} - \overline{w'^2_2}} \right). \tag{20}$$

Since the third rotation is based on a strong (and likely incorrect for complex flow) constraint on the turbulent stress, it should be used with extreme caution. Finnigan [3_7.34] recommends that the third rotation not be applied but that the general procedure should be used.

3.7.3.2 Planar Fit Method

As an alternative, Wilczak et al. [3_7.32] suggest a *planar-fit* technique to determine the pitch and roll angles of the anemometer which reduces the error associated with the second and third rotations described above. The method uses average velocity vectors from an ensemble of averaging periods to define a new best-fit *x-y* plane using multiple linear regression. This plane is defined by a pitch and roll angle with respect to the sonic anemometer coordinate system similar to that described above. This regression forces the average vertical velocity to be zero (i.e., $\overline{w}_{pf} = 0$). First, the planar-fit velocity components are determined through a partial rotation, namely

$$
\begin{Bmatrix} u_{pf} \\ v_{pf} \\ w_{pf} \end{Bmatrix} = \mathbf{T}(\psi_{pf}) \cdot \mathbf{S}(\varphi_{pf}) \cdot \begin{Bmatrix} u_m \\ v_m \\ w_m \end{Bmatrix} = \mathbf{P} \cdot \begin{Bmatrix} u_m \\ v_m \\ w_m \end{Bmatrix} , \tag{21}
$$

where, $\mathbf{P}=T(\psi_{pf})\mathbf{S}(\varphi_{pf})$ and the planar-fit pitch (φ_{pf}) and roll (ψ_{pf}) angles are determined from a least squares fitting of the mean velocity vectors to a single plain. The final rotated velocities ($\overline{u}_f \neq 0$, $\overline{v}_f = 0$ and $\overline{w}_f = 0$) are obtained by rotating the planar-fit velocities through the appropriate yaw angle θ_{pf} using Eq. (22) as follows:

$$\begin{Bmatrix} u_f \\ v_f \\ w_f \end{Bmatrix} = \mathbf{R}(\theta_{pf}) \cdot \begin{Bmatrix} u_{pf} \\ v_{pf} \\ w_{pf} \end{Bmatrix} \tag{22}$$

where,

$$\theta_{pf} = \tan^{-1}\left(\frac{\overline{v}_{pf}}{\overline{u}_{pf}} \right).$$

Here, $\overline{u}_{pf}$ and $\overline{v}_{pf}$ represent average values taken for each averaging period. To determine the planar-fit pitch (φ_{pf}) and roll (ψ_{pf}) angles [3_7.32] consider a modified version of Eq. (21) for the mean velocities that includes a mean offset error vector $\overline{a}$ associated with the error in the measured velocities associated with the instrument.

$$\begin{Bmatrix} \overline{u}_{pf} \\ \overline{v}_{pf} \\ \overline{w}_{pf} \end{Bmatrix} = \begin{bmatrix} p_{11} & p_{12} & p_{13} \\ p_{21} & p_{22} & p_{23} \\ p_{31} & p_{32} & p_{33} \end{bmatrix} \begin{Bmatrix} \overline{u}_m - a_1 \\ \overline{v}_m - a_2 \\ \overline{w}_m - a_3 \end{Bmatrix} \tag{23}$$

Wilczak et al. [3_7.32] show that the $\overline{u}$ and $\overline{v}$ biases are usually much smaller than the $\overline{w}$ bias. Consequently, their method only contains a mean offset in the vertical velocity. This is done by setting the last equation in (23) to zero (i.e., $\overline{w}_{pf} = 0$) and rearranging to obtain

$$\overline{w}_m = a_3 - \frac{p_{31}}{p_{33}}\overline{u}_m - \frac{p_{32}}{p_{33}}\overline{v}_m. \tag{24a}$$

that is,

$$\overline{w}_m = b_0 + b_1\overline{u}_m + b_2\overline{v}_m \tag{24b}$$

The *b* coefficients are then solved for by minimizing the function *S*,

$$S = \sum_{i=1}^{N} \left(\overline{w}_{m,i} - b_0 - b_1\overline{u}_{m,i} - b_2\overline{v}_{m,i} \right)^2, \tag{25}$$

where $\bar{u}_{m,i}$, $\bar{v}_{m,i}$ and $\bar{w}_{m,i}$ are the components of the mean velocities measured by the sonic anemometer for each averaging period. Taking the partial derivative of (25) with respect to b_0, b_1 and b_2 and setting the resulting equations each equal to zero yields the following system of equations:

$$
\begin{bmatrix}
N & \sum \bar{u}_{m,i} & \sum \bar{v}_{m,i} \\
\sum \bar{u}_{m,i} & \sum \bar{u}_{m,i}^2 & \sum \bar{u}_{m,i}\bar{v}_{m,i} \\
\sum \bar{v}_{m,i} & \sum \bar{u}_{m,i}\bar{v}_{m,i} & \sum \bar{v}_{m,i}^2
\end{bmatrix}
\begin{Bmatrix} b_0 \\ b_1 \\ b_2 \end{Bmatrix}
=
\begin{Bmatrix}
\sum \bar{w}_{m,i} \\
\sum \bar{u}_{m,i}\bar{w}_{m,i} \\
\sum \bar{v}_{m,i}\bar{w}_{m,i}
\end{Bmatrix}.
$$

The b_i coefficients can be easily obtained using a standard matrix inversion technique. Once they are obtained, the planar-fit pitch and roll angles are calculated using (24) and the orthogonality condition: ($p_{31}^2 + p_{32}^2 + p_{33}^2 = 1$) as follows:

$$
p_{31} = \frac{-b_1}{\sqrt{b_1^2 + b_2^2 + 1}} = -\cos\psi_{pf} \sin\varphi_{pf}
$$

$$
p_{32} = \frac{-b_2}{\sqrt{b_1^2 + b_2^2 + 1}} = -\sin\psi_{pf}
$$

$$
p_{33} = \frac{1}{\sqrt{b_1^2 + b_2^2 + 1}} = \cos\psi_{pf} \cos\varphi_{pf}
$$

$$
\sin\psi_{pf} = -p_{32} \qquad\qquad \sin\varphi_{pf} = \frac{b_1}{\sqrt{b_1^2 + 1}}
$$

$$
\cos\psi_{pf} = \sqrt{\frac{b_1^2 + 1}{b_1^2 + b_2^2 + 1}} \qquad\qquad \cos\varphi_{pf} = \frac{1}{\sqrt{b_1^2 + 1}}
$$

The planar-fit pitch and roll angles can now be substituted into (21) to solve for u_{pf}, v_{pf} and w_{pf}. The last step is to solve for the final rotated velocities using (22).

3.7.3.3 Other Sensor Issues

While, it has been observed that thermal expansion of SATs has a negligible effect on accuracy [3_7.17], the sensors and supports of SATs create wakes that interfere with the flow field being measured and result in a velocity deficit error. The aerodynamic distortion on the acoustic path is not only due to wake effects but also to blockage effects, leading to acceleration in certain parts of the acoustic path regions [3_7.30]. Horizontally mounted SATs (Fig.1c and d) are usually pointed into the mean wind and have a restricted range of permissible wind angles to avoid wakes of the sensor and mounting

equipment. Vertically mounted SATs (Fig.1a and b) are often axisymmetric but have supports that induce wake effects. Also, any mean vertical winds will cause significant flow distortion by the base. Many manufacturers include corrections that are meant for specific anemometer orientations to account for wake shadowing effects of the sensor supports. These usually assume that the mean flow is horizontal and are not valid for flow with significant mean vertical velocity components. Shadowing effects have been investigated by [3_7.36], [3_7.37], [3_7.30], [3_7.38], [3_7.39], [3_7.40] and [3_7.41]. Fig. 7 is an example of corrections that can be applied to particular SATs. With more sensors being used in environments with a non-horizontal mean flow (e.g., urban flow and complex terrain), this topic has become an important issue. In particular, [3_7.42] has shown that introducing an angle of attack to the sonic anemometer can cause large errors in mean velocities and turbulent fluxes. Additional calibration data over a full range of wind angles is necessary to alleviate this problem. It should be remarked that in extremely poor designs, certain sonic anemometer geometries may lead to undefined measured wind speed values (i.e. one measurement corresponding to multiple wind values) as it is described in [3_7.43].
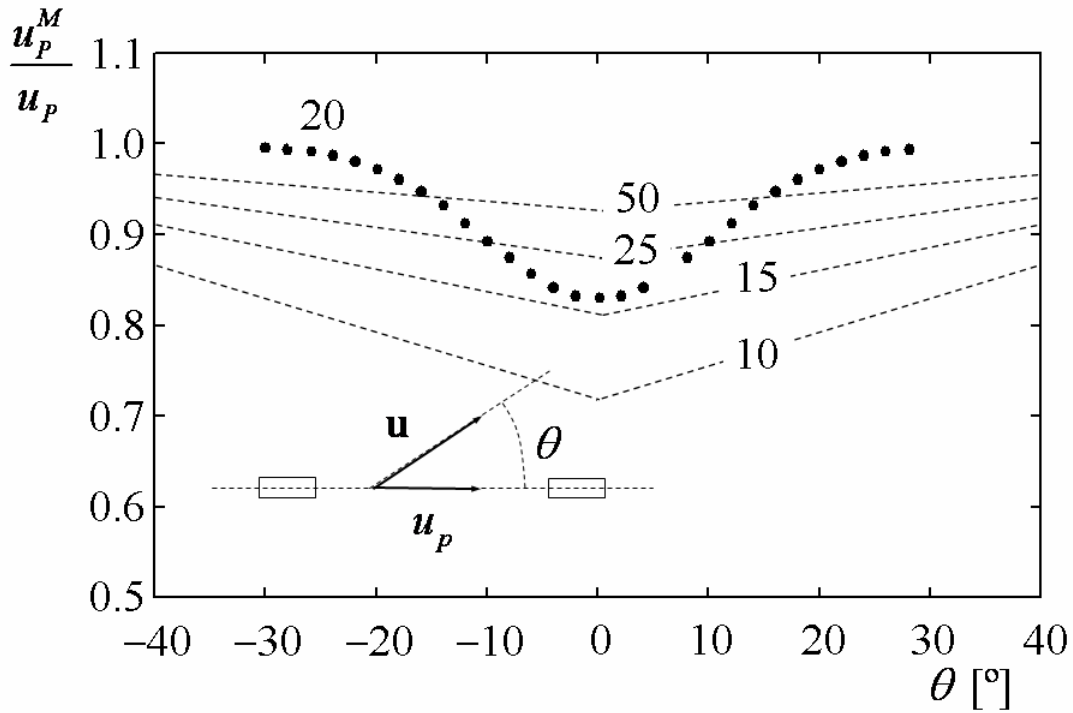

Fig. 7: Velocity attenuation, u_P^M / u_P, from transducer shadowing in a sonic anemometer (with orthogonal probe axes) shown as a function of wind direction (θ) for various values of L/a (10-50), from [3_7.20] and [3_7.36]. Here, a is the diameter of the transducer, L the separation distance between transducers, **u** is the wind vector and u_P the it projection on the path.

As shown by [3_7.23], the temperature measurements from the SAT UAT are sensitive to moisture content and cross-stream velocity and should be corrected [3_7.44]. Schotanus et al. [3_7.45] and Liu et al. [3_7.23] have proposed corrections. Some manufacturers include correction algorithms that can be run on-line or implemented in post processing. Liu et al. [3_7.23] have provided correction information for several specific types of sonic anemometers including: Campbell Scientific, Inc.'s CSAT3, Metek GmbH's USA-1 and Gill Instrument Ltd.'s Solent R2,R3,R31,HS.

3.7.4   Data acquisition Requirements

Most SATs have data acquisition electronics built into the instrument on a mounting arm or in an included electronics box. Communication with the electronics typically takes place through a modem type communication protocol using a PC terminal (e.g., via an RS-232 serial port) or a data logger. Some manufacturers use proprietary digital communication protocols (e.g., SDI for Vaisala, Inc. and SDM for Campbell Scientific, Inc.) that give the best instrument performance. These digital communication techniques allow for external instrument triggering. In addition, most manufacturers' electronics can be programmed to output analog signals.

3.7.5   Use and Calibration Procedures

One of the biggest advantages of SATs is that they typically only require an initial calibration. Usually, SATs only need to be recalibrated if the sensors have been disturbed (for example, causing the pulse path distance L to be changed). Some models require regular zeroing in a still/anechoic chamber [3_7.46, 3_7.2]. In general, prior to instrument deployment, checking the zero of the instrument in a still chamber is a good practice. If the path distance has changed, SATs are usually calibrated using a reference standard (e.g., pitot-static or hot-wire probe) in a wind tunnel. Calibration method specifications are proposed in the literature [3_7.46, 3_7.2] however, a need for a uniform systematic calibration method still exists. The calibration of a sonic anemometer involves the determination of the function $\mathbf{f}_{cal}$: $R^3 \rightarrow R^3$ for a number of different values of wind speed magnitude $\mathbf{u}$, wind direction (or horizontal incidence angle) θ and vertical angle of incidence α, which may give rise to a large number of calibration points. For example, a full typical calibration may consist of $N_u \times N_\theta \times N_\alpha = 10 \times 40 \times 10 = 4000$ calibration points. From these number of experimental relations between the real and measured wind speed vector $\{u,v,w\}$ (or equivalent vector magnitude $\{|\mathbf{u}|,\theta,\alpha\}$) a proper fit of function $\mathbf{f}_{cal}$: $R^3 \rightarrow R^3$ must be determined that can be applied to correct future measurements.

The authors have explored linear interpolation methods to reduce the information contained in the calibration test. The philosophy behind this method can be more easily illustrated if a two dimensional calibration is considered. If only the variation of two components of the wind speed are evaluated (i.e. the two horizontal components u and v), the relation between the measured and real values may be represented graphically as in Figs. 8 and 9 where the white dots represent the calibration values for the vector $\{u,v\}$

and the grey dots the corresponding measured values $\{u^M, v^M\}$ (a similar scheme with a different data process is presented in [3_7.39]).
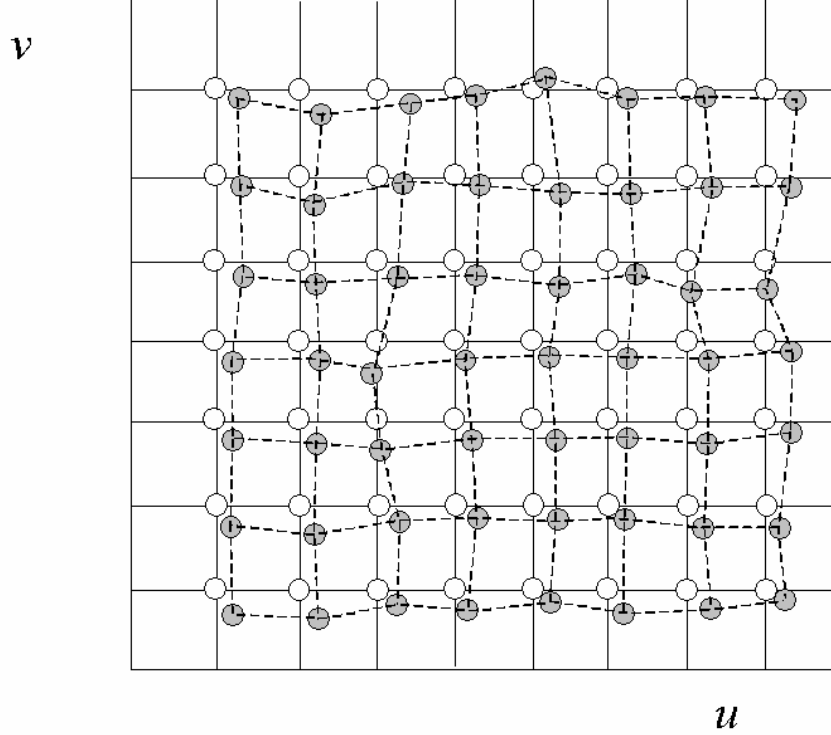

Fig. 8: Schematic of the results from a two dimensional calibration. The graphic relation $\mathbf{f}_{cal}$: $R^2 \rightarrow R^2$ is presented. The white dots represent the wind tunnel measurements (real values of u and v), whereas the grey dots represent the values measured by the sonic anemometer (measured values of u and v).

An enlargement of the schematic shown in Fig. 8 is represented in Fig. 9. The white triangle represents the interpolated (corrected after calibration) value of the measured vector $\{u^M, v^M\}$. This calibrated value is obtained in this case by a linear calibration function $\mathbf{f}^l_{cal}$: $R^2 \rightarrow R^2$ so that the corrected vector is obtained as:

$$\left(\mathbf{u}_{k,m}\right)^M_C = \left\{u^M_{k,m}, v^M_{k,m}\right\}_C = \mathbf{f}^l_{cal}\left(\mathbf{u}_{k',m'}; \mathbf{u}_{i,j}, \mathbf{u}_{i',j'}, \mathbf{u}_{i+1,j}, \mathbf{u}_{i'+1,j}...\mathbf{u}_{i'+1,j'+1}\right). \tag{26}$$

To avoid cross contamination of the velocity components, extreme care needs to be taken during mounting and leveling SATs. Over level terrain, bubble indicators are useful for leveling. However, over sloping terrain users must determine if the sensor is to be placed parallel to the slope or oriented with respect to the gravitational vector. In addition, sensors should be placed to maximize the useful range of measurements by minimizing tower and sensor distortion by orienting the sensor into the predominant wind direction. Quality control routines are used in post processing to remove or mark data with winds that have been disturbed by the tower.

Finally, wet sensors, rain, snow, icing and debris on sensors degrade the ultrasonic signal. Most manufactures have heated sensors that are intended for cold weather use to prevent icing.
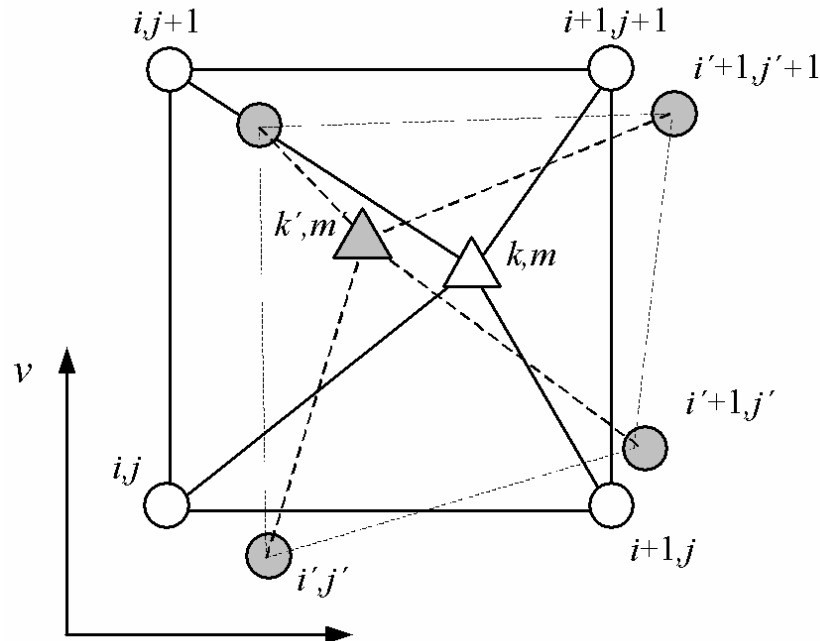

Fig. 9: Schematic of the correction process of a sonic measurement. The white dots represent the real values of the wind speed determined during calibration in wind tunnel, the grey dots represent the values of u and v measured by the sonic anemometer during calibration, the grey triangle represents the values of u and v measured in the field, and the white triangle represents the values of the interpolated (corrected after calibration) u and v.

3.7.6   Manufacturers and Costs

A number of manufacturers exist around the world including: Vaisala, Inc., RM Young Company, Applied Technologies, Inc., Campbell Scientific, Inc., Metek GmbH and Gill Instruments Ltd. Anemometer cost varies significantly. 2D SATs are less expensive than 3Ds typically costing $1-$3k. The price range of 3D SATs are approximately $2-8k. The prices generally vary with accuracy and additional sensor options and do not include data loggers or laptop computers for data storage.

3.7.7   Device Comparison

SATs provide a number of advantages for making point measurements in flows with length scales of interest that are greater than $O(1$ m$)$ and frequencies less than $O(10$ Hz$)$. Over this range, they provide much better response than traditional meteorological instruments such as cup and vane or propeller anemometers [3_7.26], [3_7.47], [3_7.1] (see Table 1). SATs are much easier to operate and much more robust than traditional

engineering laboratory equipment such as LDA, PIV or hot-wire anemometry. However, for investigating high frequency turbulence at the smallest length scales, traditional engineering laboratory equipment must be employed.

Acknowledgements:

References:

[3_7.1] Wyngaard, J: Annu. Rev. Fluid Mech. **13**, 399 (1981)

[3_7.2] VDI – Guideline (Ed.): VDI. VDI 3786, Part 12 (1994)

[3_7.3] M. Aubinet, A. Grelle, A. Ibrom, U. Rannik, J. Moncrieff, T. Foken, A.S. Kowalski, P.H. Martin, P. Berbigier, C. Bernhofer, R. Clement, J. Elbers, A. Granier, T. Grunwald, K. Morgenstern, K. Pilegaard, C. Rebmann, W. Snijders, R. Valentini and T. Vesala (Eds.): A.H. Fitter and D.G. Raffaelli, *Advances in Ecological Research*, **30**, 113 (2000)

[3_7.4] B. Duan, C.W. Fairall and D.W. Thomson: J. Appl. Meteorol. **27**, 642 (1988)

[3_7.5] B.B. Hicks, D.R. Matt and R.T. McMillen: Boundary-Layer Meteorol. **47**, 127 (1988)

[3_7.6] A. Cuerva, S. López-Díez, and D. Bercebal: James & James (Sciences Publishers) Ltd. Proceedings of the European Wind Energy Conference. ISBN: 1 902916 00 X Nice, 663 (1999)

[3_7.7] A. Fragoulis: Aerospace Sciences Meeting and Exhibit, AIAA, Reno, 33 (1997)

[3_7.8] M.W. Rotach, S.-E. Gryning, E. Batchvarova, A. Christen and R. Vogt: Meteorol. Atm. Phys. **87**, 39 (2004)

[3_7.9] N. Kato, T. Ohkuma, J.R. Kim, H. Marukawa and Y. Niihori: J. Wind Eng. Aerodyn. **88**, 67 (1992)

[3_7.10] J. Finnigan: Annu. Rev. Fluid Mech. **32**, 519 (2000)

[3_7.11] R.M. Petrone, J.S. Price, J.M. Waddington and H. Von Waldow: J. of Hydrology, **295**, 198 (2004)

[3_7.12] X. Lee, W. Massman, B. Law (Eds.): *Handbook of Micrometeorology: A Guide for Surface Flux Measurement and Analysis* (Kluwer Academic Publishers, Dordrecht 2004)

[3_7.13] D. Banfield, R. Dissly, A.D. Toigo, P.J. Gierasch, W.R. Dagle, D. Schindel, D.A. Hutchins, B.T. Khuri-Yakub: Proceedings of the 6th International Conference on Mars, 3144 (2003)

[3_7.14] A. Cuerva and A. Sanz-Andres: Journal of Geophysical Research – Planets **108**, E4, 5029, doi:10.1029/2002JE001944 (2003)

[3_7.15] H.P. Vaterlaus, T. Hossle, P. Giordano and C. Bruttin (Ed.): J.G. Webster, *Instrumentation and Sensors Handbook* (CRC Press, Boca Raton 1999)

[3_7.16] V.E. Suomi: AFCRC Tech. Report 56-274, University of Wisconsin, Dept. of Meteorology (1957)

[3_7.17] J.C. Kaimal (Eds.): F. Dobson, L. Hasse, and R. Davis, *Air-Sea Interaction – Instruments and Methods* (Plenum Press, New York 1982)

[3_7.18] H.L. Fox (Eds.): Bolt, Beranek and Newman, AFCRL-68-0180 (1968)

[3_7.19] S.E. Larson, F.W. Weller, J.A. and Businger: J. Appl. Meteorol. **18**, 562 (1979)

[3_7.20] J.C. Kaimal and J.J. Finnigan: *Atmospheric Boundary Layer Flows: Their Structure and Measurement* (Oxford University Press, New York 1994)

[3_7.21] A. Cuerva, A. Sanz-Andres: J. Wind Eng. Aerodyn. **88**, 25 (2000)

[3_7.22] J.C. Kaimal and J.E. Gaynor: Boundary-Layer Meteorol. **56**, 401 (1991)

[3_7.23] H. Liu, G. Peters and T. Foken: Boundary-Layer Meteorol. **100**, 459 (2001)

[3_7.24] A. Cuerva, A. Sanz-Andres and J. Navarro: Experiments in Fluids **34**, 345 (2003)

[3_7.25] J.C. Kaimal, J.C. Wyngaard and D.A. Haugen: J. Appl. Meteorol. **7**, 827 (1968)

[3_7.26] J.C. Kaimal (Eds.): H. Lenschow, *Probing the Atmospheric Boundary Layer* (Amer. Meteorol. Soc., Boston 1986)

[3_7.27] C. Wamser: Boundary-Layer Meteorol. **84**, 231 (1997)

[3_7.28] K. Henjes, P.K. Taylor, M.J. Yelland: J. Atmos. Oceanic Technol. **16**, 181 (1999)

[3_7.29] A. Cuerva and A. Sanz-Andres: James & James (Sciences Publishers) Ltd. Proceedings of the European Wind Energy Conference, Nice, 649 (1999)

[3_7.30] A. Wieser, F. Fielder and U. Corsmeier: J. Atmos. Oceanic Technol. **18**, 1585 (2001)

[3_7.31] A. Cuerva, A. Sanz-Andrés and S. Franchini: The Fourth European & African Conference on Wind Engineering. (Eds.): J. Náprstek & C. Ficher ITAM AS CR, Prague, Paper 152 (2005).

[3_7.32] J. M. Wilczak, S. P. Oncley, S. A. Stage: Boundary-Layer Meteorol. **99**, 127 (2001)

[3_7.33] R. Sozzi, M. Favaron: Environmental Software **11**, 259 (1996)

[3_7.34] J.J. Finnigan: Boundary-Layer Meteorol. **113**, 1 (2004)

[3_7.35] McMillan: Boundary-Layer Meteorol. **43**, 231 (1988)

[3_7.36] J.C. Wyngaard and S.-F. Zhang: J. Atmos. Oceanic Technol. **2**, 548 (1985)

[3_7.37] J.A. Murray, J.C. Klewicki and C.A. Biltoft: ASME-FED **161**, 43 (1993)

[3_7.38] A. Grelle and A. Lindroth: J. Atmos. Oceanic Technol. **11**, 1529 (1994)

[3_7.39] C. Kraan, W.A. Oost: J. Atmos. Oceanic Technol. **6**, 516 (1989)

[3_7.40] D. Heinemann, D. Langner, U. Stabe and H. Waldl (Ed.): R. Watson, European Wind Energy Conference EWEC 97. IWEA. Dublin, 409 (1998)

[3_7.41] N.G. Mortensen and J. Højstrup: Symposium of Meteorology Observation and Instrumentation, 501 (1992)

[3_7.42] M.K. van der Molen, J.H.C. Gash and J.A. Elbers: Agr. Forest Meteorol. **122**, 95 (2004)

[3_7.43] A. Cuerva, A. Sanz-Andres and O. Lopez: J. Atmos. Oceanic Technol. **21**, 1868 (2004)

[3_7.44] J. Wyngaard, J: J. Atmos. Oceanic Technol. **2**, 548 (1985)

[3_7.45] P. Schotanus, F.T.M. Nieuwstadt and H.A.R. De Bruin: Boundary-Layer Meteorol. **26**, 81 (1983)

[3_7.46] ISO 16622: 1st Edition (2001)

[3_7.47] S. Cervenka (Ed.): Energieonderzoek Centrum Nederland, ECN-I-92-029 DE92 557290 (1992)

[3_7.48] J.D. Anderson: *Modern Compressible Flow: With Historical Perspective, 2**nd Edition* (McGraw-Hill Publishing Company, New York 1990)